Acta Biomaterialia 67 (2018) 319–330

Contents lists available at ScienceDirect

Acta Biomaterialia

journal homepage: www.elsevier.com/locate/actabiomat

Full length article

The limiting layer of fish scales: Structure and properties

D. Arola [a,b,c,*], S. Murcia [b], M. Stossel [c], R. Pahuja [c], T. Linley [d], Arun Devaraj [e], M. Ramulu [c], E.A. Ossa [f], J. Wang [c]

[a] Department of Mechanics, Shanghai University, Shanghai, China
[b] Department of Materials Science and Engineering, University of Washington, Seattle, WA, USA
[c] Department of Mechanical Engineering, University of Washington, Seattle, WA, USA
[d] Energy and Environment Directorate, Pacific Northwest National Laboratory, Richland, WA, USA
[e] Physical and Computational Sciences Directorate, Pacific Northwest National Laboratory, Richland, WA, USA
[f] Production Engineering Department, School of Engineering, Universidad Eafit, Medellín, Colombia

ARTICLE INFO

Article history:
Received 27 July 2017
Received in revised form 20 November 2017
Accepted 7 December 2017
Available online 14 December 2017

Keywords:
Apatite
Armor
Collagen
Fish scales
Hardness
Ionic substitution
Limiting layer
Nature
Scale morphology

ABSTRACT

Fish scales serve as a flexible natural armor that have received increasing attention across the materials community. Most efforts in this area have focused on the composite structure of the predominately organic elasmodine, and limited work addresses the highly mineralized external portion known as the Limiting Layer (LL). This coating serves as the first barrier to external threats and plays an important role in resisting puncture. In this investigation the structure, composition and mechanical behavior of the LL were explored for three different fish, including the arapaima (*Arapaima gigas*), the tarpon (*Megalops atlanticus*) and the carp (*Cyprinus carpio*). The scales of these three fish have received the most attention within the materials community. Features of the LL were evaluated with respect to anatomical position to distinguish site-specific functional differences. Results show that there are significant differences in the surface morphology of the LL from posterior and anterior regions in the scales, and between the three fish species. The calcium to phosphorus ratio and the mineral to collagen ratios of the LL are not equivalent among the three fish. Results from nanoindentation showed that the LL of tarpon scales is the hardest, followed by the carp and the arapaima and the differences in hardness are related to the apatite structure, possibly induced by the growth rate and environment of each fish.

Statement of Significance

The natural armor of fish, turtles and other animals, has become a topic of substantial scientific interest. The majority of investigations have focused on the more highly organic layer known as the elasmodine. The present study addresses the highly mineralized external portion known as the Limiting Layer (LL). Specifically, the structure, composition and mechanical behavior of the LL were explored for three different fish, including the arapaima (Arapaima gigas), the tarpon (Megalops atlanticus) and the carp (Cyprinus carpio). Results show that there are significant differences in the surface morphology of the LL from posterior and anterior regions in the scales, and between the three species. In addition, the composition of the LL is also unique among the three fish. Results from nanoindentation showed that the LL of tarpon scales is the hardest, followed by the carp and the arapaima and the differences in hardness are related to the apatite structure, possibly induced by the growth rate and environment of each fish. In addition, a new feature was indentified in the LL, which has not been discussed before. As such, we feel this work is unique and makes a significant contribution to the field.

1. Introduction

Structural materials in nature have been increasingly studied over the last decade and they are serving as a source of inspiration in the generation of new engineered materials with advanced properties [1–3]. Nature utilizes minerals and proteins as the

* Corresponding author at: Department of Materials Science and Engineering, Roberts Hall, Box 352120, University of Washington, Seattle, WA 98195, USA.
E-mail address: darola@uw.edu (D. Arola).

https://doi.org/10.1016/j.actbio.2017.12.011
1742-7061/

primary building blocks for hard tissues and largely controls the mechanical behavior through modulation of the mineral content [4]. However, for some structural biological materials there are additional features of the microstructure that yield further improvements in performance.

Within the theme of bioinspiration, scientists have been fascinated by natural structural materials, which exhibit high specific strength and toughness [5]. Natural armors, in particular, are a special class of composite materials consisting of a matrix of collagen [4,6] or keratin fibers [7]. Fish scales have drawn considerable attention due to their laminated composite structure, their flexibility (i.e low resistance to bending) and their specific strength and toughness [8]. These qualities could have evolved to meet the specific requirements of each fish according to its habitat and predator/prey relationships.

Elasmoid scales are found on teleost fish. In comparison to the other types of scales, elasmoid scales are thin and compliant, which permits large range of motion, greater swim speeds and facilitate the multifunctional needs of propulsion and protection [9–11]. In comparison, ganoid scales are more rigid and exhibit a layered microstructure resembling that of teeth [12,13], They are much stiffer, which would appear to be designed to enhance protection. Elasmoid scales can be divided into a posterior or exposed region, and an anterior region that is mostly covered by other scales and embedded within the skin (Fig. 1A). The posterior area of the scale has a high roughness related to hydrodynamic properties during swimming [14]. In comparison, the anterior area consists of grooves in the radial direction (radii) and ridges that form circular rings (circuli) around a central area called the "focus" [15]. The radii and circuli of scales possibly provide increased flexibility and a means of maintaining the scale attachment, respectively [11]. While these morphological features would be expected to possess geometry important to function, a quantitative comparison of these external features among fish of different species has not been reported.

The overall structure of elasmoid scales consists of three distinct layers across the thickness (Fig. 1B). The Limiting layer (LL) is the most external and highly mineralized region of the scale and has been regarded as the first barrier against penetration [11]. Based on earlier studies [16–18], the LL is a mineral matrix with randomly dispersed thin (30–50 nm in diameter) collagen fibers. The mineralization front extends from the LL into the underlying elasmodine, which is a laminate consisting of discrete plies of unidirectionally aligned collagen fibers with a diameter of between 100 and 160 nm [9,17]. The plies are rotated at specific angles with respect to one another and exhibit a thickness that is dependent on the fish [8]. The elasmodine can be divided into two discrete layers, including the external elasmodine (EE) and the internal elasmodine (IE), which are differentiated only by the lower mineral content of the later.

The LL is clearly a key layer of the structure of elasmoid scales. It is in direct contact with the environment and would be expected to have additional functions beyond simply contributing to the penetration resistance [11]. Understanding the limiting layer and its functions could contribute to biomimetic designs for abrasion resistant coatings, surface treatments of engineered composites, etc. However, there is less detailed knowledge on the structure and properties of the LL from elasmoid scales in comparison to the elasmodine. In addition, no study has compared the composition and properties of the LL for scales of fish across species or from different habitats. Therefore, the objective of the present study is to characterize the LL of scales from selected species of fish for the first time, and to extend the current knowledge of this mineral system. The focus of this evaluation it the morphology of the scales, their composition, and the corresponding mechanical properties.

2. Materials and methods

Elasmoid scales were harvested from the bodies of three different fish including the *Cyprinus carpio* (i.e. freshwater carp), the *Megalops atlanticus* (i.e. tarpon), and the *Arapaima gigas* (i.e. pirarucú). For simplicity, these three fish are referred to as the carp, the tarpon and the arapaima, respectively. Scales from these three fish were selected for evaluation due to the differences in locomotion and habitat, which could contribute to the development of unique structure and properties of the LL. In addition, the scales from these three fish have received the most attention in the engineering and materials science literature. The carp represents the control for this study as they are raised within a controlled aquatic environment. Being raised in captivity, this fish has no natural predators and special needs for locomotion or protection. The tarpon and the arapaima were wild fish captured in the Caribbean

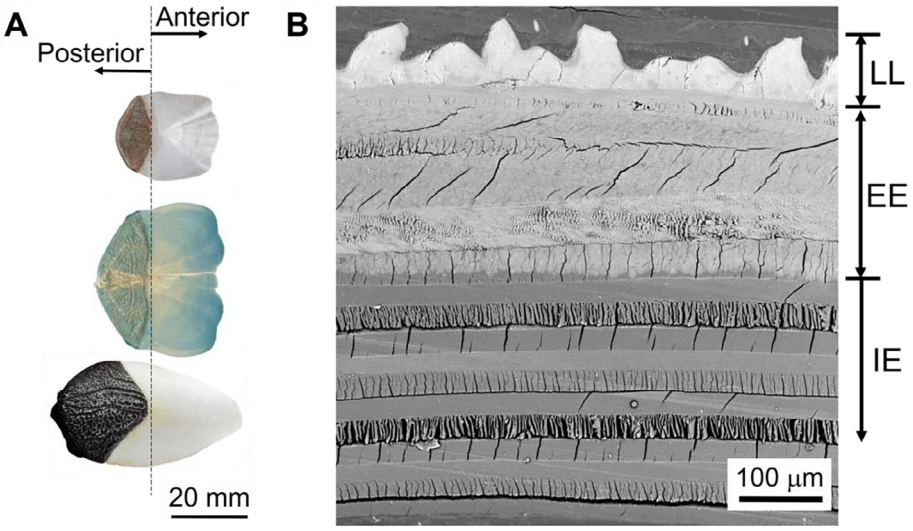

Fig. 1. Scales of the carp, tarpon and arapaima. A) Relative geometry and size of the scales, as well as identification of the anterior and posterior regions of the scales. The anterior is the part of the scale that is embedded beneath other scales, which is towards the head, and the posterior is the part which is exposed and oriented towards the tail. B) SEM image of the cross-section of a representative tarpon scale denoting the three distinct regions including the limiting layer (LL), external elasmodine (EE) and internal elasmodine (IE). The differences in grayscale between these three regions is attributed to the differences in mineral content, including highest in the LL and lowest in the IE.

Sea and the Amazon River, respectively. The tarpon inhabits both fresh and salt waters of the Atlantic. With a top speed of near 7 kph it is one of the ten fastest fish of the world. Speed is important for evading predators and feeding. Lastly, the arapaima is one of the largest freshwater fish in the world and inhabits the Amazon River Basin in South America. Each fish inhabits a different natural environment, and has unique protective requirements. One difference worth noting among the three fish was their size. According to their weight (3.4, 5.5 and 20 kg, respectively) and length (53, 75 and 157 cm, respectively), the fish ranged between 3 and 6 years of age.

The scales were extracted from the body of each fish within three characteristic regions, namely the head, middle and tail regions. These regions corresponded to distances from the gill plate of 15%, 40% and 80% of the total number of scales along the lateral line, respectively. The extraction was performed by hand and achieved by gentle pulling of the scale. After extraction, the scales were stored in Hanks Balanced Salt Solution (HBSS) at room temperature. The scales from each fish were divided into two groups, including one for evaluating external features of the LL (topography), and one for evaluating properties over the cross-section including chemistry and hardness.

The external topography of the limiting layer was evaluated using a surface profilometer (MarSurf XR 20, Göttingen, Germany) with skidless contact probe and 2 μm diameter. Surface profiles were obtained perpendicular to the circuli ridge line within the anterior and posterior regions of selected scales. These profiles were acquired using a traverse length of 10 mm. The surface profiles were used in calculating the peak to valley height (Ry) and wavelength of the circuli within selected windows of evaluation distributed across the total length of the scales. In addition, the microscopic features of the surfaces were evaluated via scanning electron microscopy (SEM) in secondary electron imaging mode (JEOL, model JSM-6010PLUS/LA, Peabody, MA). The samples were sputtered with Au/Pd to facilitate prior to the SEM evaluation.

Within a week of extraction the scales selected for cross sectional analysis were fixed in 2% glutaraldehyde buffered with 0.1 M sodium cacodylate with pH = 7.2 for 4 h. They were then rinsed in 0.1 M sodium cacodylate buffer followed by post-fixation in 1% osmium tetroxide buffered with 0.1 M sodium cacodylate for 2 h. After rinsing, the scales were dehydrated through an ascending ethanol series from 50 to 95%, followed by 100% of acetone and instant dehydration in 2,2-dimethoxypropane (DMP) for 5 h. Instant dehydration and rinsing with 100% acetone was followed by infiltration of the scales in Mollenhauer resin.

To evaluate the structure and composition across the thickness, selected scales were cross-sectioned and then faced with a microtome using a glass knife (Leica EM UC6 Ultramicrotome, Vienna, Austria). Raman spectroscopy was performed with a Renishaw inVia system equipped with a Leica DMIRBE inverted optical microscope (Renishaw, Wotton-under-Edge, United kingdom) utilizing a 785 nm Diode laser (50% power) in backscattering configuration to quantify the chemical composition and the distribution of mineral content. The instrument was calibrated to the Stokes Raman signal at 785 cm^{-1} using a bulk single crystal of Si with the direction oriented normal to the laser. A 50 aperture was used with pinhole, resulting in an approximately 2 μm diameter sampling cross section. The spectral samples were collected over 20 s exposure time and were carried out through the thickness of the limiting layer of head scales over an equidistant distribution of evaluation points. The number of points ranged from three to six, according to the limiting layer thickness. The Raman peaks were used to determine the modes of vibration of the phosphate and collagen. To quantify the mineral stoichiometry, X-ray photoelectron spectroscopy (XPS) experiments were performed using a Kratos Axis Ultra DLD photoelectron spectrometer (Manchester, UK) operated with a monochromatic Al Kα X-ray source (*HV* = 1486.6 eV) at 20 mA and 15 kV. The surfaces were briefly sputtered with 5 keV argon ions prior to analysis. High resolution imaging was performed in parallel imaging mode at field of view 1 or 2 (800 or 400 mm) with single point background corrections recorded at binding energies 10 eV below the corresponding peak. High-resolution O 1s, N 1s, C 1s, P 2p and Ca 2p spectra were acquired with an analyzer pass energy of 160 eV with a data point spacing of 0.5 eV/step at field of view 2. Measurement locations where distributed across the LL of each fish with a spot size of 15 μm.

Preliminary information on the atomic distribution of trace elements in the LL layers was also detected by Atom Probe Tomography (APT). Samples were prepared using the dual-beam SEM/FIB instrument (Helios Nanolab, FEI, Hillsboro, Oregon) using established protocols [19]. A rectangular coating of platinum (FIB-Pt) of roughly 2×15 μm was deposited over a region of interest on the polished cross-section using the ion beam (30 kV, 46 pA). A wedge of material below the Pt coating was cut out and sequentially affixed to the tops of Si posts in an array (Cameca Scientific Instruments, Madison, WI) with FIB-Pt and a final width of 1–2 μm. Each tip was shaped and sharpened using annular milling patterns of increasingly smaller inner and outer diameters. The majority of the amorphized surface region and implanted gallium in the tip surface was removed by milling at 2 kV, 24 pA. The APT analyses were conducted in a Cameca local-electrode atom-probe tomograph (LEAP 4000XSi, Cameca, Madison, WI) using a pulsed laser (λ = 355 nm, 100 kHz, 100 pJ per pulse). The DC potential on a microtip during APT was controlled to maintain an evaporation rate of 0.0025 or 0.005 ions per laser pulse. The base temperature of the microtip was maintained at 60 K and the ambient vacuum pressure was below 10^{-8} Pa.

Nanoindentation was performed to evaluate the mechanical properties of the LL as a function of depth, which could be different between fish as a result of the LL composition and differences in LL thickness. The experiments were performed using an Ubi1 nanomechanical test instrument (Hysitron, Inc., MN) and a Berkovich indenter with 150 nm tip radius. Indentations were performed after ascending ethanol treatment using a conventional trapezoidal loading scheme including a 10 s loading period, 5 s hold at maximum load and 10 s unloading. Hardness values were obtained from the maximum load, divided by the indentation area, and the reduced elastic modulus was obtained from the indentation stiffness at unloading versus indentation depth curve, following the Oliver and Pharr method [20]. Indents were made over the LL thickness in increments of 10 μm for the carp and every 15 μm for the tarpon and arapaima. An array of 6 indents were performed at each point to obtain the average hardness and elastic modulus values. In addition, scanning probe microscopy (SPM) images of the cross-sectional topography were obtained using the *in situ* scanning capability of the nanoindenter to ascertain the quality of indents and features of interest identified using the optical microscope.

Lastly, the moment of inertia (first moment of area) was calculated for the scale geometry of all three fish, to better understand the effects of the differences in their cross-section geometry and the elastic modulus variations across the thickness. The moment of inertia was calculated for flexure of the scales about the axis perpendicular to the longitudinal axis of the fish. Estimates were obtained for scales from the head, middle and tail regions of each fish, and according to the geometry of the scale within the mid-anterior region. The calculations were conducted for the composite layer construction, which included the section thickness of the internal and external elasmodine, the LL cross-section, and the elastic moduli for each of these regions, which were obtained from nanoindentation. The geometry of the LL was modeled according to

the section profiles obtained from profilometry, as well as the base LL thickness beneath the circuli.

An evaluation of the quantitative measures of the LL characteristics was conducted to identify significant differences using a two-way Analysis of Variance (ANOVA) and Tukeys HSD test. Significance differences were identified by $p \leq 0.05$.

3. Results

3.1. Morphology

The surface morphology of the limiting layer from scales of the three fish is shown in Fig. 2. Most prominent in these figures are

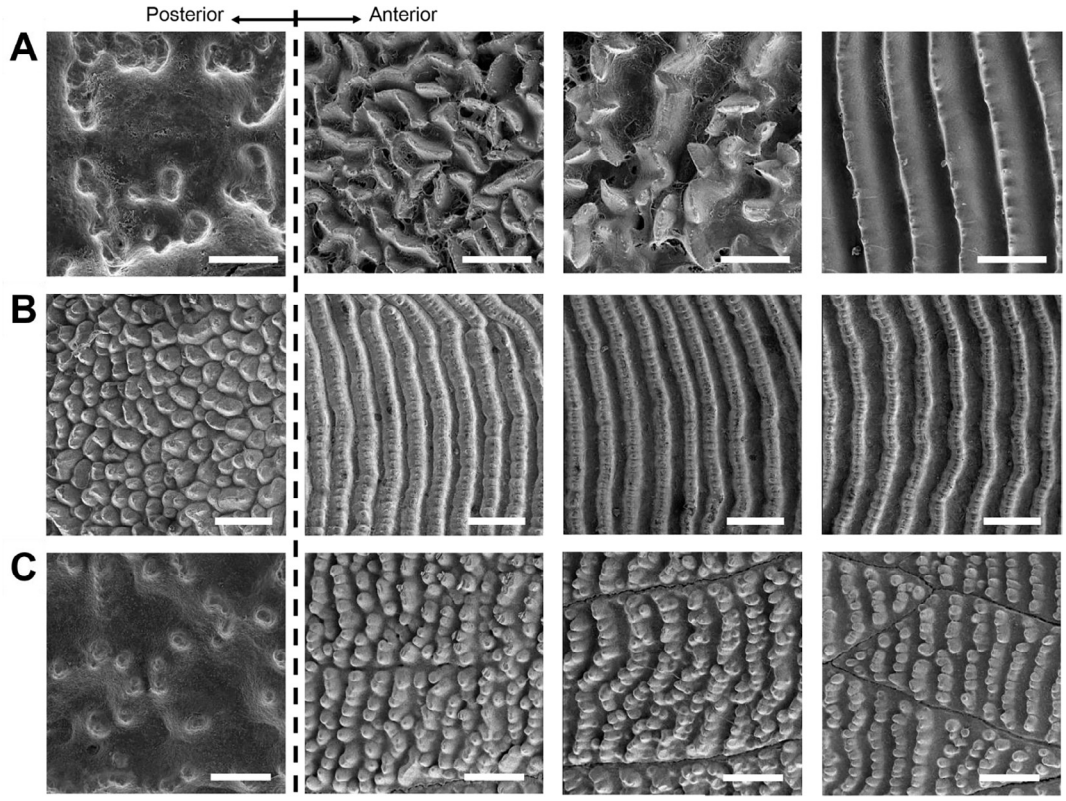

Fig. 2. The surface morphology of the limiting layer seen from top (external) view. The images were obtained at normalized distances from the posterior edge of the scale including (from left to right) 15%, 30%, 50%, and 70% of the total length. Note that the locations of anterior and posterior across the scale surface are shown in Fig. 1. A) Carp scales, scale bar = 5 μm; B) tarpon scales, scale bar = 200 μm, C) arapaima scales, scale bar = 500 μm. The lines evident in these scales are portions of the scale radii that extend from the focus.

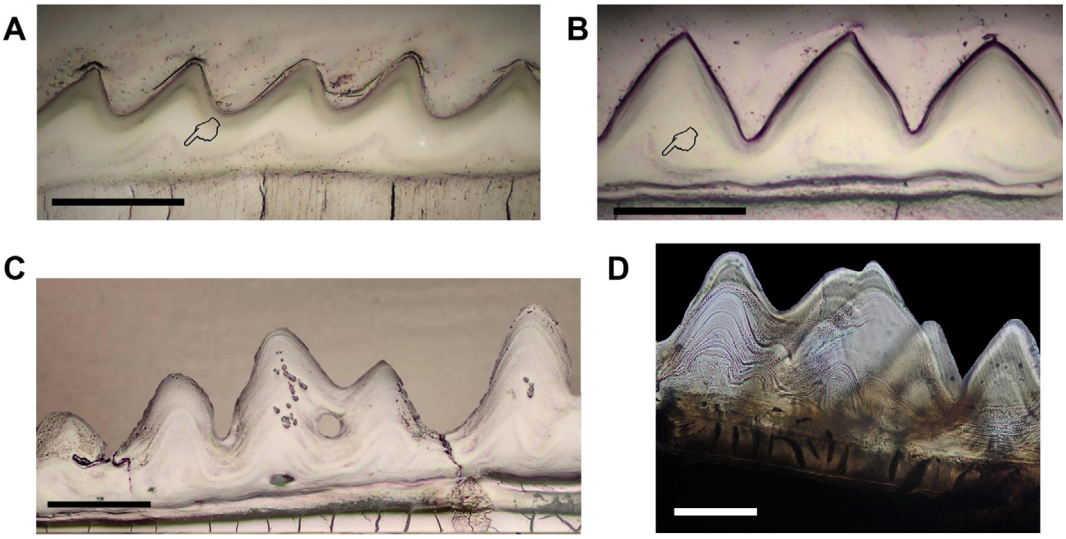

Fig. 3. Optical images of the limiting layer for the three fish for A) carp (scale bar 50 μm), B) tarpon (scale bar 50 μm) and C) arapaima (scale bar 200 μm) scales. Note that the LL of the arapaima scales has a cross sectional wave pattern that is clearly seen in D) transmitted optical light image of the arapaima LL (scale bar 100 μm). Transition zones indicated in Figures A and B (pointers) were noted between the mineralized limiting layer and the mineralized collagen matrix for the carp and tarpon scales.

the circuli, which are the continuous mineralized ridges that extend vertically in these images, particularly in those for the anterior region of the tarpon. Differences in both the geometry and spacing of the circuli are evident between the three species in both the anterior and posterior regions. In general, the posterior region does not exhibit continuous mineralized circuli, but rather exhibits protrusions with no particular pattern. For the carp (Fig. 2A), an array of irregular shaped protrusions covers the exposed region of the scales, which transitions to ridges after the posterior/anterior (P/A) interface. For cycloid scales, including scales of the carp, it is common for dispersed denticles to begin around the focus of the scale [21]. Anterior to the focus, progressive agglomeration and fusion form longer and more uniform ridges in circuli from the anterior region of the scale. In the tarpon scales, the posterior region is uniformly covered by tightly packed circular protrusions (Fig. 2B). At the P/A interface, the circular protrusions transition into ridges; with proximity to the anterior edge, the separation distance between the ridges increases, with each protrusion becoming more clearly distinguishable. For the arapaima (Fig. 2C), protrusions are also evident and have a rounded morphology that changes from the posterior to anterior regions. In the posterior

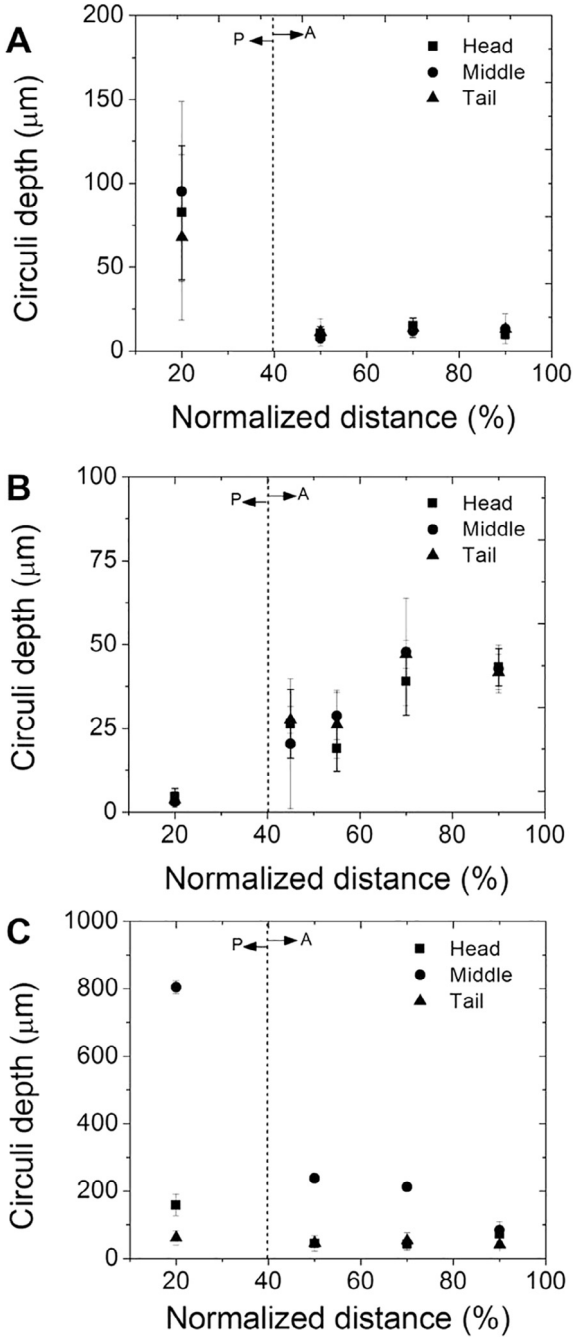

Fig. 4. A comparison of the average circuli depth for the LL over the total length of scales from the posterior edge. The distributions are shown for the three anatomical positions of the A) carp, B) tarpon and C) arapaima scales. There are significant differences between the anterior (A) and posterior (P) regions of the scales for all three fish. Note that scales of the arapaima have the highest peak to valley height in their surface profile.

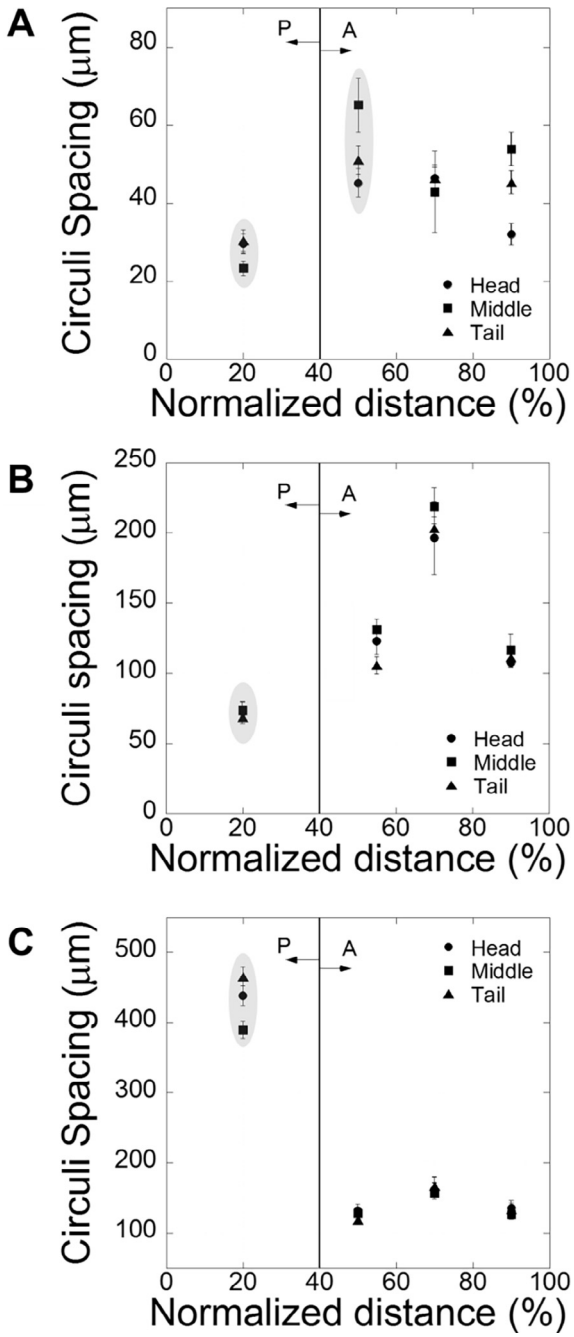

Fig. 5. A comparison of the circuli spacing on the LL surface of scales from the A) carp, B) tarpon and C) arapaima in the three anatomical positions. There are significant differences in the spacing between the three fish and also between regions. The highlighted data represents spacing distinguished from the protrusions and not continuous circuli.

region, the protrusions are rounded and randomly dispersed. After the P/A interface the protrusions have a tear shape and are arranged in rows. In comparing the LL morphology of the three fish, it is interesting that the tarpon scales have the most continuous ridges, whereas the circuli of the arapaima are limited to individual protrusions.

Selected optical micrographs for representative cross-sectioned scales of the three fish are shown in Fig. 3. These images are focused on the LL within the anterior region to accentuate details of the circuli geometry. For the carp (Fig. 3A) and the tarpon (Fig. 3B), the cross sectioned LL exhibits a serrated pattern due to the distribution of the circuli and their geometry. The average LL thickness of the carp and tarpon scales from the LL/EE interface to the circuli peaks is roughly 40 μm and 70 μm, respectively. For the arapaima, the LL exhibits a much more irregular cross section geometry due to the tear shaped protrusions (Fig. 2C). Nevertheless, the average LL thickness (peak to LL/EE interface) is roughly 300 μm.

There are unique features of the LL from the three fish. For example, in the carp scales there is a transition zone between the highly mineralized LL and the EE (Fig. 3A). This zone is located nearest the EE and follows a serrated pattern that is in phase with the circuli. As evident in Fig. 3A, both the external circuli and the transition are inclined towards the anterior direction, having an inclination of approximately 70° with the surface. Notably sharper than the carp, the circuli of the tarpon were not inclined (Fig. 3B), and the apparent depth of the valleys in the circuli is greater than in the carp (Fig. 3A). There is a transition zone evident between the LL and EE of the tarpon scales as well, and it is slightly out of phase with the LL profile. The LL of the arapaima scales is much more irregular (Fig. 3C) in height distribution, which results from the assembly and distribution of mineral protrusions. In addition, there are concentric waves evident in the cross section that resemble the marks generated by waves on a beach; they are in-phase with the circuli of the LL. These features can be better appreciated in the transmitted light image in Fig. 3D from a section of approximately 400 μm thickness. The vertical distance between these wave-like features decreases with increasing proximity to the LL/EE interface. Near the outer edge of the LL the average separation spacing of the waves is

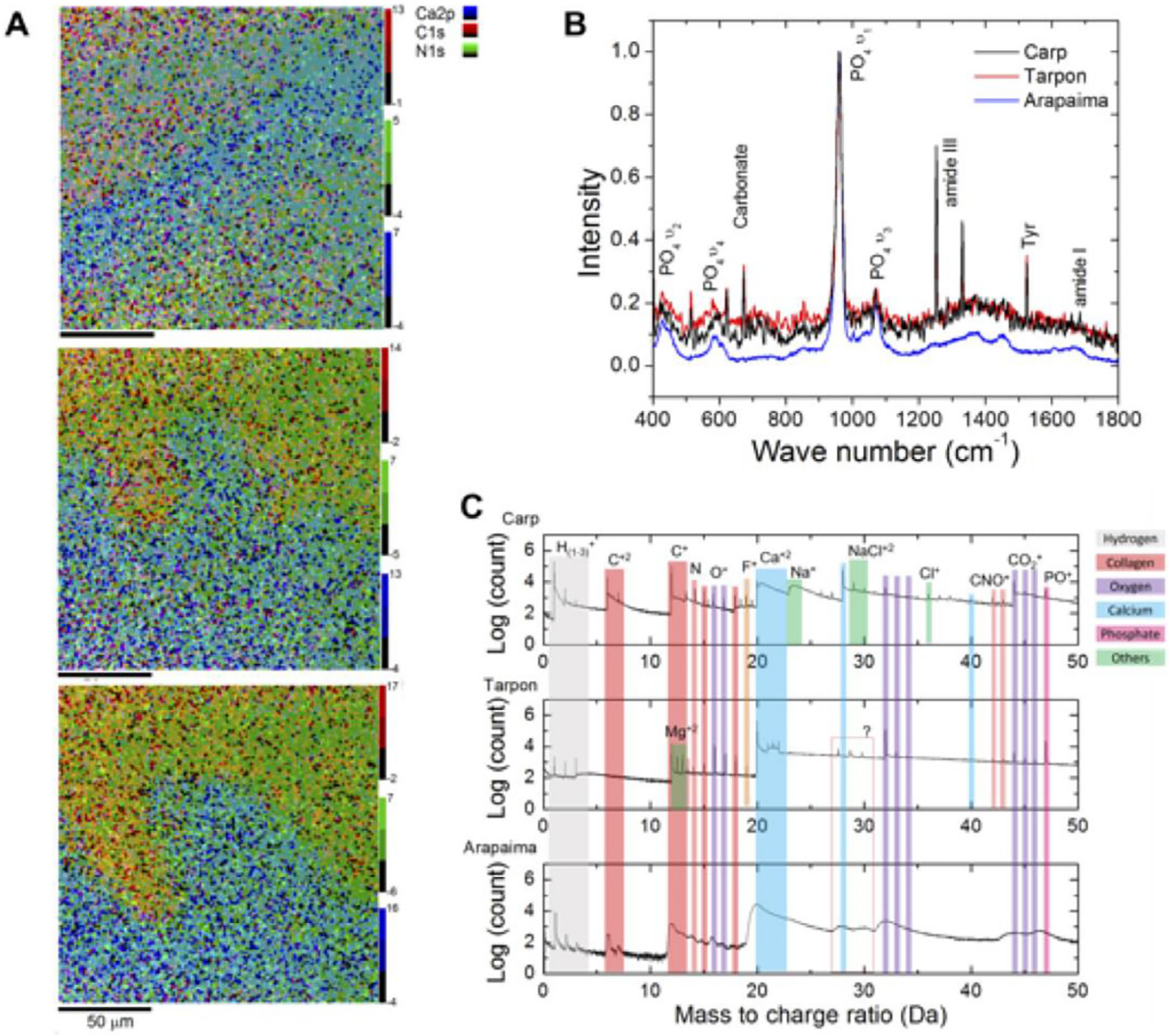

Fig. 6. Evaluation of the limiting layer composition in head scales A) Element distribution across the thickness of the LL from XPS analysis. Shown, top to bottom are the carp, tarpon and arapaima. The areas with high concentrations of nitrogen (green) correspond to resin used for the scale mount. B) Raman and C) APT spectra of the limiting layer at 0.5 normalized distance. Differences in B) are related to the changes in the apatite structure. The atomic scale evaluation of the elemental composition in C) detected small amounts of Mg in the tarpon scales and ions of NaCl on the carp, elements that facilitate the mineralization process. (For interpretation of the references to colour in this figure legend, the reader is referred to the web version of this article.)

roughly 10 μm, and that decreases to almost no distinct wave feature near the interface with the EE.

As evident from surface views in Fig. 2 and the cross-section images in Fig. 3, the LL exhibits an interesting external surface morphology. To achieve an objective comparison, the surface topography of the scales was quantified in terms of the circuli depth and circuli spacing. Results for the Circuli Depth (CD) are presented in Fig. 4 for scales from the three regions of each fish. For the carp scales (Fig. 4A) there is a significant ($p \leq 0.05$) decrease in CD from the posterior region to the P/A interface, after which the CD remained constant in the anterior region of the scales. The CD of the tarpon scales is shown in Fig. 4B and shows the significant increase in CD from posterior to anterior regions. Results for the CD for the arapaima scales are shown in Fig. 4C and show that there is a general decrease in CD from the posterior to the anterior regions. Although there were no differences in the CD with respect to anatomical position for the carp and tarpon, the LL of the arapaima exhibited significant differences with location, especially for the posterior zone of scales of the middle region. (Fig. 4C). The LL of scales from the head and middle regions decreased from the posterior to the anterior regions, whereas there was no spatial variation in the LL for the circuli of scales from the tail. It is important to note that there were substantial differences in the maximum CD between the three fish. The maximum CD in order of decreasing depth was found in scales of the arapaima (~800 μm), carp (~100 μm) and tarpon (~50 μm).

Results for the Circuli Spacing (CS) measurements of scales from the carp, tarpon and arapaima are shown in Fig. 5A to C, respectively. Clearly evident in this figure, there are differences in the CS between the three fish. For the carp and tarpon the smallest spacing was identified in the posterior region, while for the arapaima scales it was found in the anterior region. Yet, no significant differences were found with respect to the anatomical region of the scales. Trends in CS for scales of the tarpon (Fig. 5B) are similar to those of the carp, i.e. the CS increases towards the anterior edges. However, in the case of the tarpon a local maximum is found at 80% of the scale length, followed by a sharp decrease at the anterior edge. The trend in CS of the arapaima scales (Fig. 5C) contrasts with that of the tarpon, with largest CS near the posterior edge and decreases with distance towards the anterior region. In general, the values range from roughly 400 μm to 200 μm, which agrees with the earlier findings [22].

3.2. Composition

Fig. 6 shows a summary of the elemental composition of the LL from scales of the head region from each fish. These results are representative of those for the entire fish. No significant differences in the mineral composition of the LL were found with respect to anatomical position of the scale [23]. Chemical distribution maps including calcium (Ca 2P), carbon (C1s) and nitrogen (N1s) across the LL thickness are shown in Fig. 6A. There was a decrease in the concentration of calcium from the outer surface of the LL to the LL/EE interface for all three fish examined. For the arapaima scales, the volume percent of apatite decreased from 60% to 40%, while the tarpon and carp scales showed a decrease from 70% to 20%. Representative Raman spectra for each fish are shown in Fig. 6B and a summary of the spectra identified is listed in Table 1. The Raman peaks with greatest intensity are attributed to phosphate, carbonate and collagen and the secondary peaks are related to amino acids [24–26]. The ν_1 phosphate stretching vibration at 961 cm^{-1} is the strongest marker for the apatite. The ν_2 and ν_4 phosphate bending vibrations were also visible at 431 cm^{-1} and 589 cm^{-1}, respectively. As evident from the review of spectra, there are differences in the apatite structure, crystallinity and collagen in the LL between the three fish. Most evident, the arapaima has a different apatite structure in comparison to the carp and tarpon, which have a strong band at 1075 cm^{-1} indicating type B carbonate substitution (carbonate substituting for phosphate in the apatite lattice). Furthermore, there are important changes with respect to the collagen structure represented by the amide I (~1677 cm^{-1}) and amide III (~1256 cm^{-1}) peaks. Broad bands were observed in the amide III (~1253 and 1325 cm^{-1}) [27–32] for the arapaima, while for the carp and the tarpon these peaks were narrow and well-defined.

Preliminary results from APT regarding the atom scale composition of the LL is shown in Fig. 6C. APT has high resolution at low concentrations, allowing the detection of trace elements like fluorine with the expected phosphates and carbonates that correspond to apatite. Interestingly, magnesium was only found in the tarpon scales, while sodium and chlorine were identified in the carp scales.

3.3. Mechanical behavior

Nanoindentation was performed to evaluate the mechanical properties of the LL and results are shown in Fig. 7. The distribution in reduced modulus with normalized distance across the LL of the three fish is shown in Fig. 7A; the modulus decreases with increasing distance from the surface for all three fish. In recognition that the LL is a biological material, the LL could exhibit spatial variations within a scale. To address possible variations, multiple indentation scans were made across the thickness of the LL in adjacent circuli ridges and results are shown for the reduced modulus of the arapaima scales in Fig. 7B. As evident in this figure, there were no significant differences between measurements at the same relative depth, indicating a high degree of repeatability. A comparison of the hardness distribution over the normalized LL thickness is shown in Fig. 7C and the distributions with physical distance are presented in Fig. 7D. Interestingly, the hardness of the arapaima LL is lower than that of the tarpon and carp scales near the outer surface, which is most evident from the normalized distribution (Fig. 7C). The largest hardness for the arapaima was 1.4 GPa, which

Table 1
Raman lines and their assignments. *v*: stretching coordinate; *d*: deformation coordinate; γw: wagging coordinate; γt: twisting coordinate; s: strong; m: medium; w: weak; sh: shoulder; vw: very weak.

Arapaima	Tarpon	Carp	Assignment
	383 s	385 s	
394 vw	397 s	397 s	Pro [21]
431 s	431 m	431 m	PO_4 ν_2 [28]
	512 m	513 m	ν(SS); cysteine [26]
584 s	580 vw	581 w	PO_4 ν_4 [27]
609 sh m			PO_4 ν_4 [28]
	621 m	622 m	PO_4 ν_4 [28]
		647 w	Phe [21]
	671 m	672 m	ν_4 CO_3^{2-}; carbonate [24,29]
851 m sh	853 vw	853 vw	Pro [21]
960 s	960 s	961 s	PO_4 ν_1 [24]
1002 w		1002 vw	ν(cc); Phe [26]
1039 vw	1033 vw	1035 w	PO_4 ν_3 [29]
	1068 m sh	1068 m	CO_3 [24,28]
1071 m	1071 m	1071 m	PO_4 ν_3 [28]
1111 m sh			ν(C-N) [21]
1187 m sh			Tyr [21]
1245 m sh			amide III [26]
	1251 s	1252 s	amide III [26]
	1330 s	1331 s	Desmosine [27]
1345 m sh			γ *w* (CH_3, CH_2) [21]
1376 m	1376 w	1374 vw	Proteoglycans (PGs) [25]
1450 s	1450 w	1447 m	C–H bending [27]
	1525 s	1524 s	Tyr [22]
1608 s		1605 vw	amide I [26]
1673 s	1674 w	1670 w	amide I [27]

is comparable to previous results that range between 1 GPa and 2 GPa [10,33]. Furthermore, the gradient in hardness across the thickness is consistent for the three fish in normalized distance, but very unique when examined in physical distance. Clearly the gradient in hardness and elastic modulus distributions are inversely proportional to LL thickness and therefore are greatest in the carp and tarpon as evident in Fig. 7D.

The flexibility of the scale is influenced by the thickness of the limiting layer, its distribution in elastic modulus and the circuli geometry. Nevertheless, the external elasmodine ratio and the number of mineralized plies in the scales must also be taken into account. Using simple mechanics of materials [34], and the previously reported data for the elasmodine ratios [8], it is possible to demonstrate the effect of microstructure and modulus variations on the scale flexibility. The moment of inertia of the scales for the three fish are shown in Fig. 8. As evident in this figure, there are spatial changes in the moment of inertia of the scales. The carp and arapaima scales undergo a decrease in the moment of inertia from the head to the tail, with 15% and 67% decrease, respectively. Meanwhile, the tarpon scales undergo an increase in moment of inertia of 15% from the head to the tail. Some of this change is related to the LL thickness and the neutral axis shift, and the remainder is attributed to the presence and shape of the mineralized protrusions.

4. Discussion

Recent investigations concerning the mechanical behavior of fish scales have established that the puncture resistance [11] and toughness [35,36] are largely dependent on the contribution of the more highly mineralized layers, namely the LL and EE. Although the distribution in mineral content over the whole scale thickness has been studied [21,37,38], to the authors' knowledge a detailed evaluation of the limiting layer has not been reported. Here, the morphology, chemical composition and mechanical properties of the limiting layer of three different fish species were evaluated and compared.

Important differences in scale structure have been found across the body of fish, which are potentially attributed to the body motion during undulatory propulsion [8,39]. Previous studies have identified a rough pattern of mineral on the surface of the scales formed by protrusions in the posterior region and by radii and circuli in the anterior region. Significant differences in the roughness have been related to the hydrodynamic characteristics and the flexibility the fish needs for its locomotion [11,22,39–41]. For instance, scales from the bluegill sunfish (*Lepomis macrochirus*) were found to have the highest radii counts from regions of the body that are either naturally curved (dorsal) or experience higher lateral curvature during swimming [42]. Circuli depth in the poste-

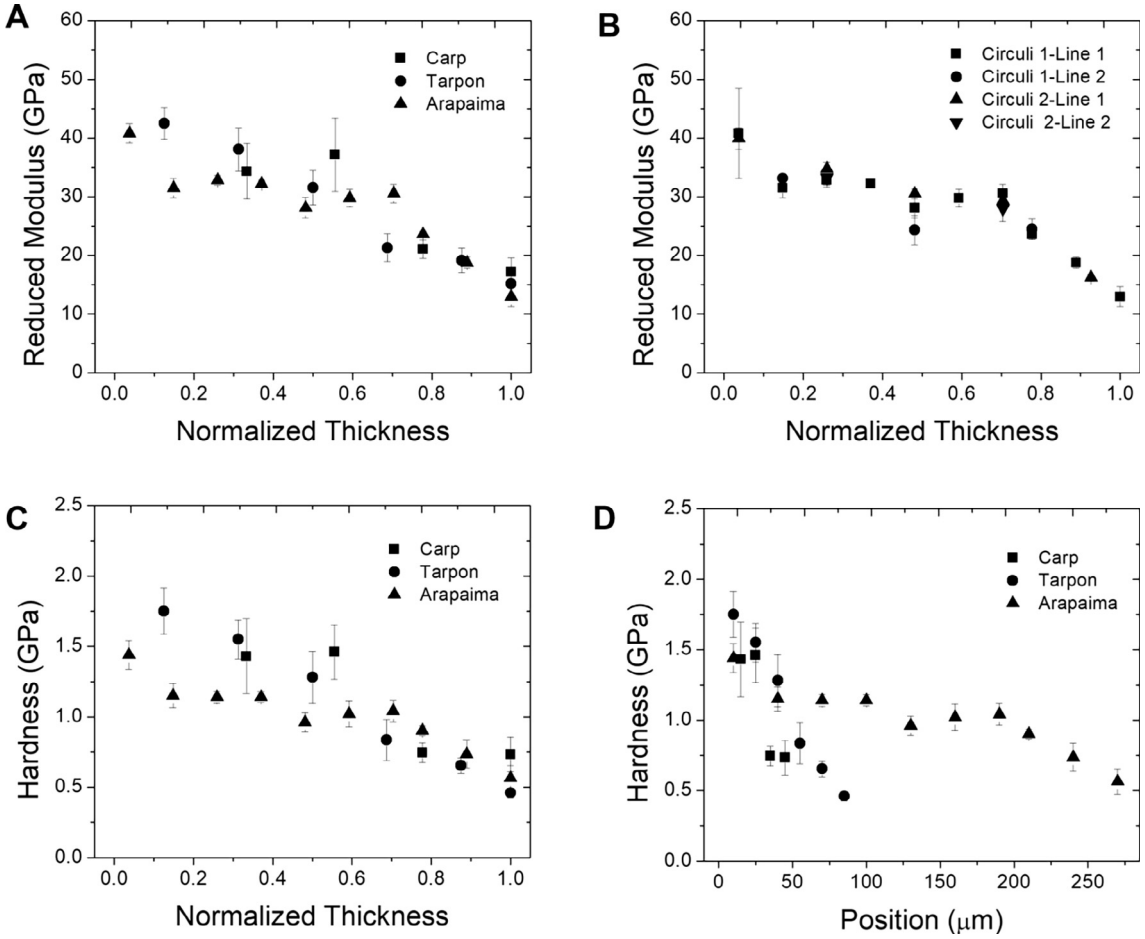

Fig. 7. Mechanical properties across the LL thickness for representative scales from the head region of the carp, tarpon and arapaima. A) Distribution of reduced modulus over the normalized thickness for the three fish and B) reproducibility of measurements for the Arapaima along different circuli. Line 1 and Line 2 represent two different analysis paths over the limiting layer for a specific scale, and Circuli 1 and Circuli 2 represent two different circuli regions that were analyzed. These results are almost identical, and show the consistency in measurements across the limiting layer for multiple locations, which were representative of measures obtained for all three fish. C) Distribution of hardness over the normalized thickness. The hardness distribution for the three fish are shown in terms of the actual thickness in D). The normalized thickness starts at the outer surface of the LL (Norm. Thickness = 0) and proceeds to the inner surface (LL/EE interface (Norm. Thickness = 1)).

rior area of scales is closely related to the boundary layers that can be formed during swimming. Due to the high amplitudes during the undulatory motion of the tail at high speed, a change from a laminar to a turbulent boundary layer can occur. Furthermore, turbulent boundary layers can form closer to the head as fish become larger [43]. For the arapaima, a fish with subcarangiform locomotion (undulation of the body involves less than one full wavelength) and significantly larger body length, the presence of higher protuberances in the posterior region (Fig. 3) could reduce drag and the potential for acoustic noise [44]; that quality increases its stealthiness. Furthermore, as the natural undulatory movement of the arapaima involves a larger portion of the body, a higher tendency to form a turbulent boundary layer is expected in mid-body of the fish. This could explain the significant increase in the circuli depth for middle scales in the posterior region in the arapaima.

The radii and the circuli spacing have been interpreted to increase the flexibility of the scales and to limit tensile stresses to the valleys between circuli during bending of the scale via the periodic reduced thickness [14,22,42]. An earlier study showed that the thickness of the LL varies within species and for instance, in the case of the arapaima scales, it also differs when compared among anatomical regions [8]. That variation is a contributing factor to the changes in scale stiffness across the body, as represented by the moment of inertia distributions in Fig. 8, and the differences between the three fish evaluated. Although some of the variation is due to the LL thickness and the neutral axis shift, the remainder is attributed to the presence and shape of the protrusions. It is interesting to note the differences in the moment of inertia distributions between the three fish species (Fig. 8), and the implications to the resistance in body flexure.

Optical images of cross-sectioned scales from the arapaima showed wave-like patterns in the LL similar to beach marks (Fig. 5D), which are similar to those in Torres et al [45]. The mineralization of scales is a cellular process that begins at the LL with the interfibrillar nucleation of crystals that cluster following a spheritic mineralization until a highly mineralized matrix is formed [17,46].

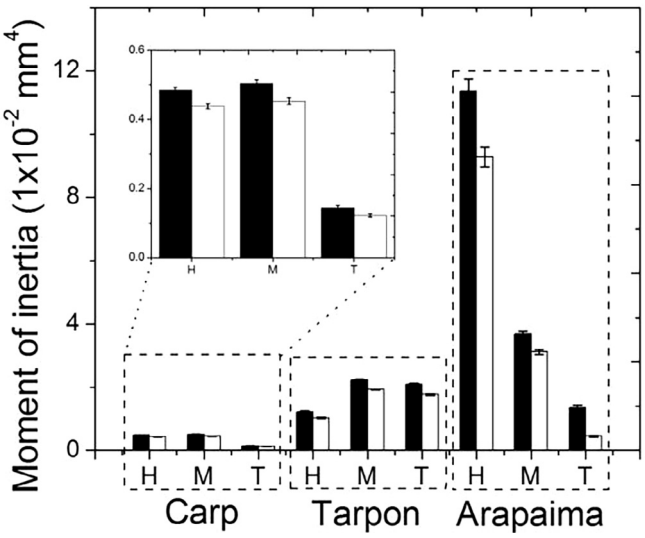

Fig. 8. Comparison of the moment of inertia for scales of the carp, tarpon and arapaima scales from the three regions. The black and white bars represent the estimates of the moment of inertia assuming a uniform thickness of the limiting layer (without circuli) and accounting for the circuli and sawtooth profile, respectively. H, M and T represent the estimates for scales of the head, middle and tail, respectively. Note the differences in spatial variations between the tarpon with respect to the carp and arapaima, which are related to the protrusions of the limiting layer.

Then, mineralization progresses to the EE, where apatite platelets organize in the c-direction of the collagen fibers, creating a reinforcement similar to that in bone [47,48]. Whether the wave-like pattern represents a change in the environment, age, or both is unclear. Since arapaima are tropical fish, it could reflect a change in seasons, food availability or diet [49]. Differences in the apatite

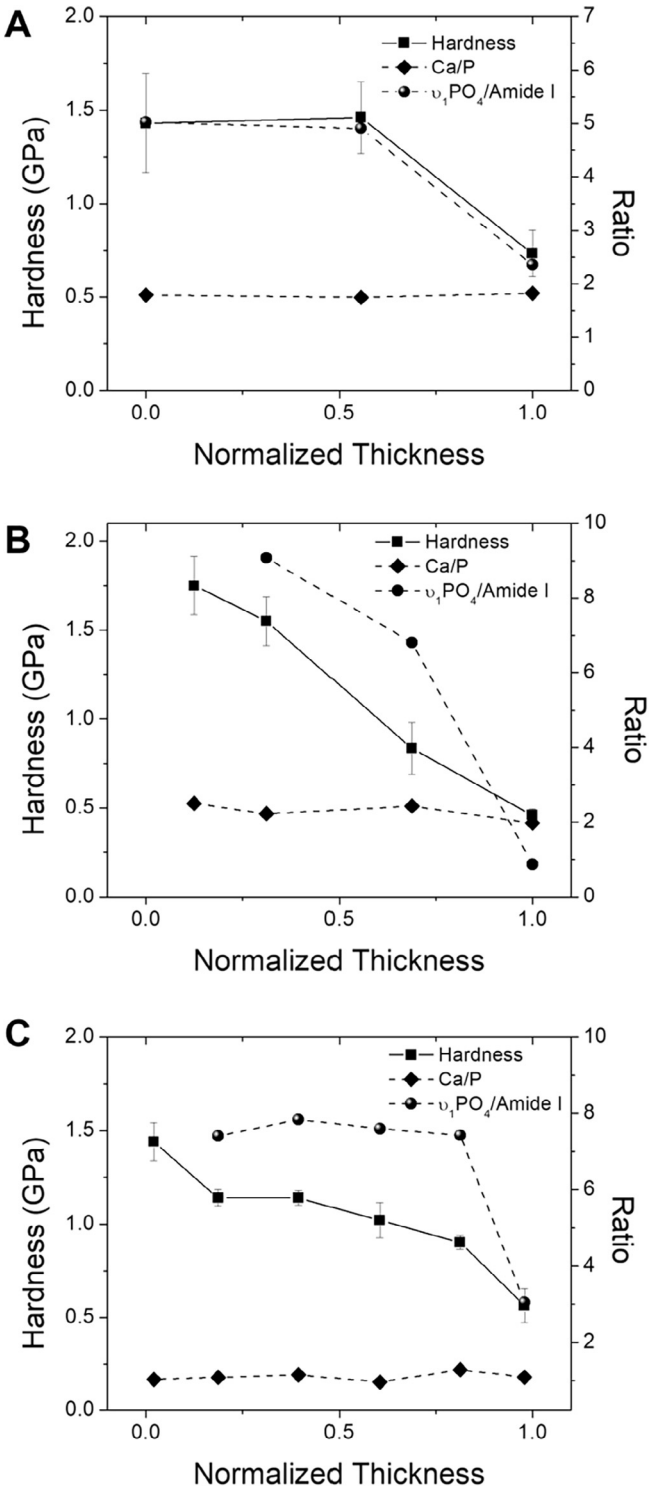

Fig. 9. Variation in the hardness, calcium to phosphate ratio (Ca/P) and phosphate/collagen ratio (ν_1PO_4/ Amide I ratio) of the limiting layer across its thickness defined in terms of the normalized thickness. A) Carp, B) Tarpon and C) Arapaima. The decrease in degree of mineralization is reflected by the decrease of the phosphate/collagen ratio as defined by the ν_1PO_4/Amide I ratio.

generated via seasonal growth patterns would be expected to be reflected as a systematic variation of elemental concentrations from the top to the bottom of the LL. However, our current results do not show such variation (Fig. 6). Ultrastructure studies of fish scales have shown that mineralization of the LL occurs by agglomeration of crystals, but there is no evidence of preferential orientations of apatite crystals in the LL [17,50,51].

Apatite accommodates chemical substitutions that change the mineral structure. As a result, there are critical effects on mineral properties, such as solubility, hardness, thermal stability, and optical properties like birefringence. Among the substituting ions reported in bone and tooth mineral are F, Cl, Na^{+}, K^{+}, Fe^{2+}, Zn^{2+}, Sr^{2+}, Mg^{2+}, citrate, and carbonate [52]. Although, not common, analyzing the mineral composition in fish scales as a non-lethal substitute for otoliths analysis has been used to obtain life history profiles during their migratory patterns. The use of spectroscopy techniques that allow high resolution profiles of elements in the cross section of scales, like laser ablation ICP-MS, demonstrated that is possible to detect changes in Mg, P, Ca, Mn, Sr and Ba in the mineral of tarpon scales [38]. Preliminary results from the APT on the LL of scales revealed differences in elements that can form ionic substitution in the apatite structure (Fig. 6A). The APT mass spectra were consistent with previous studies of HAP [19,53,54], however C ions and CN ions were also detected in the LL due to the presence of collagen and non collageneous proteins. The mass spectra for the arapaima shows signs of attenuation, for instance in the C^{+} and the Ca^{2+} regions, which demonstrate differences in the energy absorption with respect to the carp and tarpon. Wild tarpon were found to have presence of Mg in their scales [38], similar to the results in Fig. 6A. Previous APT studies on enamel have shown the presence of interfaces enriched with Mg and Na between HAP nanowires [54], which have an effect on the solubility at the periphery and result in anisotropic etching [53]. Furthermore, the presence of Na and Cl in carp scales could be a result of the brackish environment related to its farming or as a result of the scales serving as reservoirs for these elements. Further study is required to obtain additional complementary understanding.

Recent studies of scales from the carp [23] and tarpon [40] have shown that there are progressive decreases in the mineral content from the LL to the IE. In scales of the arapaima, this decrease was responsible for spatial changes in hardness and elastic modulus throughout the thickness of the scale [10,33]. There are also changes in these properties over the thickness of the LL. Fig. 9 shows the distribution in hardness, mineral/organic ratio and Ca/P ratio over the LL thickness for head scales from the three fish. The mineral to organic ratio was estimated from the areas of the peaks corresponding to ν_1 PO_4 and Amide I. The distributions in Fig. 9 reveal that the gradient in LL hardness is most correlated with the degree of mineralization, as expected.

Further exploration of the LL hardness and dependence on composition in Fig. 10 show that while a lower mineral to organic ratio results in a reduction in hardness of the LL, similar values of hardness can be achieved by significantly different values of the mineral to collagen ratio (Fig. 10A). To understand the differences in the LL hardness between fish (Fig. 7), it is necessary to analyze if the LL is composed by the same type of apatite crystals. A comparison between the Ca/P of the three fish with the measured hardness is presented in Fig. 10B. Theoretical stoichiometric HA has a 1.67 Ca/P ratio [31,52,55] with an average hardness of 1.5 ± 0.5 GPa [56]. This value becomes important as higher Ca/P are related to higher hardness. A higher Ca/P implies a higher strain in the crystal lattice, which will have a direct effect on the physical properties of the apatite. It is evident that the tarpon has the highest Ca/P, being followed by the carp and arapaima. An increase or decrease in the Ca/P with respect to stoichiometric HA is a reflection of ionic substitutions [21,53]. According to the Ca/P ratio, each fish is composed of different apatites, being respectively calcium deficient carbonated apatite, tetracalcium phosphate (TetCP) and tricalcium phosphate (TCP) for the carp, tarpon and arapaima scales, respectively [31,52]. Therefore, an ascending contribution from TCP, HA, calcium deficient carbonated apatite and TetCP is expected on hardness.

Previous Raman studies on arapaima scales found the presence of carbonate anions in its apatite structure [10,22]. Nevertheless, in the present results, peaks related to the vibration of carbonates were only found in carp and tarpon scales. The presence of carbonates is possibly related to the fish habitat. Carbonated HA has also been reported in the scales of northern snakehead (*Channa argus)* and red sea bream *(Pagrus major),* fish that similar to the tarpon are found in the sea [21,26]. Fig. 6C revealed the presence of Na and Cl in the composition of the carp's LL, suggesting that it may have been farmed in an environment involving brackish water. Without further study these comments are speculative. However, they do emphasize the importance of knowing the origins of fish in future studies.

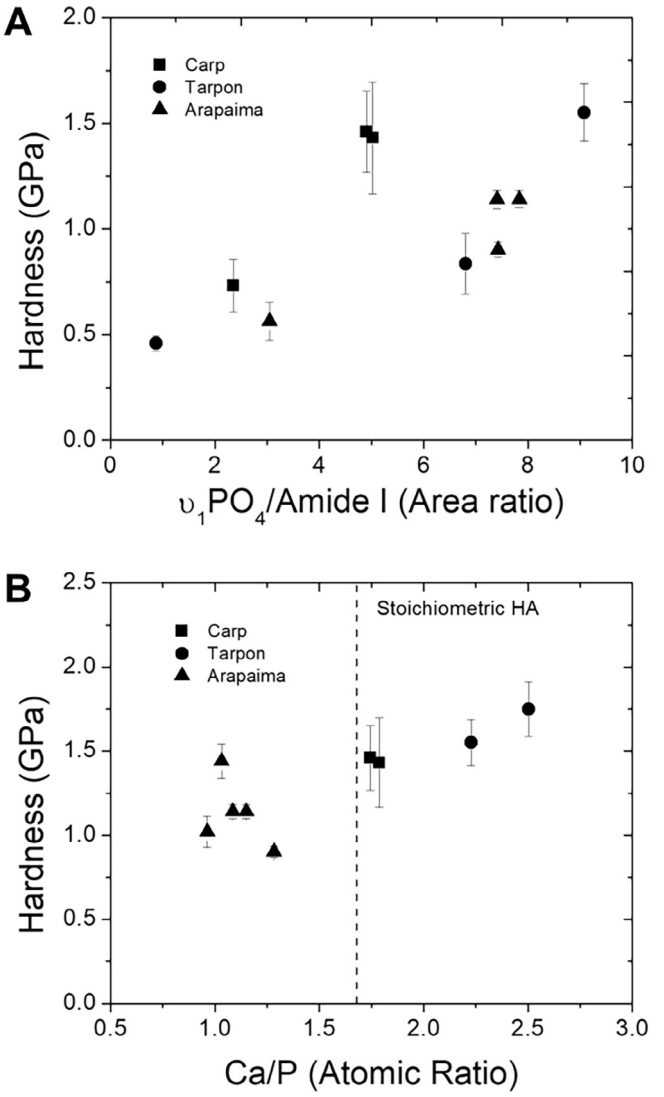

Fig. 10. Hardness of the limiting layer and its dependence on the degree of mineralization and apatite structure for the carp, tarpon and arapaima scales. A) Hardness variation with mineralization reflected by the phosphate to collagen ratio, and B) Hardness variation with apatite structure reflected by the calcium to phosphate ratio.

Results from this investigation provide new understanding concerning the mineral structure of the LL and their contribution to changes in properties of the scales from three different species of fish. Additionally, important morphological features in the LL of carp and arapaima scales were seen for the first time. To better understand the wave-like pattern in the circuli of arapaima scales, a characterization enabling high-resolution elemental variations across the LL thickness is needed. The mechanics of scaled skins and their multi-functionality is a topic of recent interest [57–59]. An increased understanding of the LL should contribute to these and future efforts. Furthermore, one of the most intriguing aspects of natural composites is how materials with such different elastic modulus can be so strongly integrated without undergoing separation. The exciting discovery of a transition zone between the LL/EE in the carp warrants further exploration of this suture-like interface and its function.

5. Conclusion

An experimental evaluation of the morphology, chemical composition and mechanical properties of the limiting layer was performed for scales of three different fish species. Significant differences in the surface morphology of circuli between the posterior and anterior regions were found in the carp, tarpon and arapaima scales. Higher protrusions were found in the posterior region of the arapaima scales in comparison to the rest of the fish, which appear related to the locomotion pattern and size of this ancient fish. A decrease in hardness and elastic modulus was identified with increasing proximity to the LL/EE interface for all three fish, and was found related to the spatial variation in the degree of mineralization. The LL of the tarpon scales was the hardest, followed by the carp and the arapaima. A positive correlation between the hardness and Ca/P ratio was identified. Results suggest that carbonate substitution of the phosphate in the apatite structure changes the Ca/P ratio and can lead to differences in the mechanical properties of the scale. Whether that is an approach used to achieve required multifunctionality, including controlled stiffness and toughness of the scales, requires further study.

Acknowledgements

This research was supported in part by a seed grant from the University of Washington, by Colciencias of Colombia through contract 0210-2013 and from a laboratory directed research and development funding associated with Chemical Imaging Initiative at Pacific Northwest National Laboratory. Furthermore, part of this work was conducted at the Molecular Analysis Facility, a National Nanotechnology Coordinated Infrastructure site at the University of Washington which is supported in part by the National Science Foundation [grant ECC-1542101], the University of Washington (UW), the Molecular Engineering & Sciences Institute and the Clean Energy Institute of the UW, and the National Institutes of Health.

References

[1] F. Barthelat, Biomimetics for next generation materials, Philos. Trans. R. Soc. London A Math. Phys. Eng. Sci. 365 (2007) 2907–2919.
[2] M.A. Meyers, P.-Y. Chen, A.Y.-M. Lin, Y. Seki, Biological materials: structure and mechanical properties, Progr. Mater. Sci. 53 (2008) 1–206.
[3] C. Ortiz, M.C. Boyce, Bioinspired structural materials, Science 319 (2008) 1053–1054.
[4] J.D. Currey, The design of mineralised hard tissues for their mechanical functions, J. Exp. Biol. 202 (1999) 3285–3294.
[5] R.K. Chintapalli, M. Mirkhalaf, A.K. Dastjerdi, F. Barthelat, Fabrication, testing and modeling of a new flexible armor inspired from natural fish scales and osteoderms, Bioinspiration Biomimetics 9 (2014) 036005.
[6] W. Yang, I.H. Chen, B. Gludovatz, E.A. Zimmermann, R.O. Ritchie, M.A. Meyers, Natural flexible dermal armor, Adv. Mater. 25 (2013) 31–48.
[7] B. Wang, W. Yang, V.R. Sherman, M.A. Meyers, Pangolin armor: overlapping, structure, and mechanical properties of the keratinous scales, Acta Biomater. 41 (2016) 60–74.
[8] S. Murcia, E. Lavoie, T. Linley, A. Devaraj, E.A. Ossa, D. Arola, The natural armors of fish: a comparison of the lamination pattern and structure of scales, J. Mech. Behav. Biomed. Mater. (2016).
[9] A.M.C. Garrano, G. La Rosa, D. Zhang, L.-N. Niu, F. Tay, H. Majd, D. Arola, On the mechanical behavior of scales from Cyprinus carpio, J. Mech. Behav. Biomed. Mater. 7 (2012) 17–29.
[10] Y. Lin, C. Wei, E. Olevsky, M.A. Meyers, Mechanical properties and the laminate structure of Arapaima gigas scales, J. Mech. Behav. Biomed. Mater. 4 (2011) 1145–1156.
[11] D. Zhu, C.F. Ortega, R. Motamedi, L. Szewciw, F. Vernerey, F. Barthelat, Structure and mechanical performance of a "modern" fish scale, Adv. Eng. Mater. 14 (2012) B185–B194.
[12] P. Allison, J. Deang, A. Diaz, A. Poda, J. Hoover, M. Horstemeyer, E. Perkins, Characterization of paddlefish (Polyodon spathula) rostrum stellate bones, Bioinspired Biomimetic Nanobiomater. 3 (2013) 63–68.
[13] B.J. Bruet, J. Song, M.C. Boyce, C. Ortiz, Materials design principles of ancient fish armour, Nat. Mater. 7 (2008) 748–756.
[14] Y. Sire, J. Géraudie, F. Meunter, L. Zylberberg, On the origin of ganoine: histological and ultrastructural data on the experimental regeneration of the scales of Calamolchthys calabaricus (osteichthyes, brachyopterygii, polypteridae), Am. J. Anatomy 180 (1987) 391–402.
[15] L.A. Jawad, Comparative morphology of scales of four teleost fishes from Sudan and Yemen, J. Nat. Hist. 39 (2005) 2643–2660.
[16] J.-Y. Sire, A. Huysseune, Formation of dermal skeletal and dental tissues in fish: a comparative and evolutionary approach, Biol. Rev. 78 (2003) 219–249.
[17] D.L. Zylberberg, G. Nicolas, Ultrastructure of scales in a teleost (Carassius auratus L.) after use of rapid freeze-fixation and freeze-substitution, Cell Tissue Res. 223 (1982) 349–367.
[18] L. Zylberberg, Collagen and mineralization in the elasmoid scales, in: Biology Intervertebrate Lower Vertebrate Collagens, Springer, 1985, pp. 457–463.
[19] L.M. Gordon, L. Tran, D. Joester, Atom probe tomography of apatites and bone-type mineralized tissues, ACS Nano 6 (2012) 10667–10675.
[20] W.C. Oliver, G.M. Pharr, An improved technique for determining hardness and elastic modulus using load and displacement sensing indentation experiments, J. Mater. Res. 7 (1992) 1564–1583.
[21] W. Liu, Y. Zhang, G. Li, Y. Miao, X. Wu, Structure and composition of teleost scales from snakehead Channa argus (Cantor)(Perciformes: Channidae), J. Fish Biol. 72 (2008) 1055–1067.
[22] M. Meyers, Y. Lin, E. Olevsky, P.-Y. Chen, Battle in the Amazon: Arapaima versus piranha, Adv. Eng. Mater. 14 (2012) B279–B288.
[23] S. Murcia, G. Li, M. Yahyazadehfar, M. Sasser, A. Ossa, D. Arola, Effects of polar solvents on the mechanical behavior of fish scales, Mater. Sci. Eng. C 61 (2016) 23–31.
[24] B.G. Frushour, J.L. Koenig, Raman scattering of collagen, gelatin, and elastin, Biopolymers 14 (1975) 379–391.
[25] V.A. Iconomidou, M.E. Georgaka, G.D. Chryssikos, V. Gionis, P. Megalofonou, S.J. Hamodrakas, Dogfish egg case structural studies by ATR FT-IR and FT-Raman spectroscopy, Int. J. Biol. Macromol. 41 (2007) 102–108.
[26] T. Ikoma, H. Kobayashi, J. Tanaka, D. Walsh, S. Mann, Physical properties of type I collagen extracted from fish scales of Pagrus major and Oreochromis niloticas, Int. J. Biol. Macromol. 32 (2003) 199–204.
[27] A. Awonusi, M.D. Morris, M.M. Tecklenburg, Carbonate assignment and calibration in the Raman spectrum of apatite, Calcified Tissue Int. 81 (2007) 46–52.
[28] S. Gamsjaeger, K. Klaushofer, E.P. Paschalis, Raman analysis of proteoglycans simultaneously in bone and cartilage, J. Raman Spectrosc. 45 (2014) 794–800.
[29] M. Gkasior-Glogowska, M. Komorowska, J. Hanuza, M. Mkaczka, A. Zajkac, M. Ptak, R. Bkedziski, M. Kobielarz, K. Maksymowicz, P. Kuropka, et al., FT-Raman spectroscopic study of human skin subjected to uniaxial stress, J. Mech. Behav. Biomed. Mater. 18 (2013) 240–252.
[30] M. Kazanci, H. Wagner, N. Manjubala, H. Gupta, E. Paschalis, P. Roschger, P. Fratzl, Raman imaging of two orthogonal planes within cortical bone, Bone 41 (2007) 456–461.
[31] S. Koutsopoulos, Synthesis and characterization of hydroxyapatite crystals: a review study on the analytical methods, J. Biomed. Mater. Res. 62 (2002) 600–612.
[32] G. Penel, G. Leroy, C. Rey, E. Bres, MicroRaman spectral study of the PO4 and CO3 vibrational modes in synthetic and biological apatites, Calcif. Tissue Int. 63 (1998) 475–481.
[33] F. Torres, E. Le Bourhis, O. Troncoso, J. Llamoza, Structure-property relationships in Arapaima Gigas scales revealed by nanoindentation tests, Polym. Polym. Compos. 22 (2014) 369–374.
[34] R.C. Hibbeler et al., Mechanics of Materials, Prentice Hall Inc, New Jersey, 2000.
[35] A.K. Dastjerdi, F. Barthelat, Teleost fish scales amongst the toughest collagenous materials, J. Mech. Behav. Biomed. Mater. 52 (2015) 95–107.
[36] S. Murcia, M. McConville, G. Li, A. Ossa, D. Arola, Temperature effects on the fracture resistance of scales from Cyprinus carpio, Acta Biomater. 14 (2015) 154–163.
[37] T. Ikoma, H. Kobayashi, J. Tanaka, D. Walsh, S. Mann, Microstructure, mechanical, and biomimetic properties of fish scales from Pagrus major, J. Struct. Biol. 142 (2003) 327–333.

[38] M. Seeley, N. Miller, B. Walther, High resolution profiles of elements in Atlantic tarpon (Megalops atlanticus) scales obtained via cross-sectioning and laser ablation ICP-MS: a literature survey and novel approach for scale analyses, Environ. Biol. Fishes 98 (2015) 2223–2238.
[39] M. Spinner, M. Kortmann, C. Traini, S.N. Gorb, Key role of scale morphology in flatfishes (Pleuronectiformes) in the ability to keep sand, Sci. Rep. 6 (2016).
[40] S. Gil-Duran, D. Arola, E. Ossa, Effect of chemical composition and microstructure on the mechanical behavior of fish scales from Megalops Atlanticus, J. Mech. Behav. Biomed. Mater. 56 (2016) 134–145.
[41] F.J. Vernerey, F. Barthelat, On the mechanics of fishscale structures, Int. J. Solids Struct. 47 (2010) 2268–2275.
[42] D.K. Wainwright, G.V. Lauder, Three-dimensional analysis of scale morphology in bluegill sunfish, Lepomis macrochirus, Zoology 119 (2016) 182–195.
[43] E.J. Anderson, W.R. Mcgillis, M.A. Grosenbaugh, The boundary layer of swimming fish, J. Exp. Biol. 204 (2001) 81–102.
[44] P.J. Hart, J.D. Reynolds, Handbook of Fish Biology and Fisheries, John Wiley & Sons, 2008.
[45] F. Torres, O. Troncoso, J. Nakamatsu, C. Grande, C. Gomez, Characterization of the nanocomposite laminate structure occurring in fish scales from Arapaima gigas, Mater. Sci. Eng. C 28 (2008) 1276–1283.
[46] F.J. Meunie, Spatial organization and mineralization of the basal plate of elasmoid scales in osteichthyans, Am. Zool. 24 (1984) 953–964.
[47] E.A. McNally, H.P. Schwarcz, G.A. Botton, A.L. Arsenault, A model for the ultrastructure of bone based on electron microscopy of ion-milled sections, PLoS One 7 (1) (2012) e29258.
[48] H.P. Schwarcz, E.A. McNally, G.A. Botton, Dark-field transmission electron microscopy of cortical bone reveals details of extrafibrillar crystals, J. Struct. Biol. 188 (2014) 240–248.
[49] L.A. Colling, C.E. Bemvenuti, M.S. Gandra, Seasonal variability on the structure of sublittoral macrozoobenthic association in the Patos Lagoon estuary, southern Brazil, Iheringia, Série Zool. 97 (2007) 257–262.
[50] A. Schönbörner, G. Boivin, C. Baud, The mineralization processes in teleost fish scales, Cell Tissue Res. 202 (1979) 203–212.
[51] L. Zylerberg, Collagen and mineralization in the elasmoid scales, in: Biology Intervertebrate Lower Vertebrate Collagens, Springer, 1985, pp. 457–463.
[52] B. Wopenka, J.D. Pasteris, A mineralogical perspective on the apatite in bone, Mater. Sci. Eng. C 25 (2005) 131–143.
[53] L.M. Gordon, M.J. Cohen, K.W. MacRenaris, J.D. Pasteris, T. Seda, D. Joester, Amorphous intergranular phases control the properties of rodent tooth enamel, Science 347 (2015) 746–750.
[54] A. La Fontaine, A. Zavgorodniy, H. Liu, R. Zheng, M. Swain, J. Cairney, Atomic-scale compositional mapping reveals Mg-rich amorphous calcium phosphate in human dental enamel, Sci. Adv. 2 (2016) e1601145.
[55] W. Suchanek, M. Yoshimura, Processing and properties of hydroxyapatite-based biomaterials for use as hard tissue replacement implants, J. Mater. Res. 13 (1998) 94–117.
[56] C. Tang, P. Uskokovic, C. Tsui, D. Veljovic, R. Petrovic, D. Janackovic, Influence of microstructure and phase composition on the nanoindentation characterization of bioceramic materials based on hydroxyapatite, Ceram. Int. 35 (2009) 2171–2178.
[57] F.J. Vernerey, F. Barthelat, Skin and scales of teleost fish: simple structure but high performance and multiple functions, J. Mech. Phys. Solids 68 (2014) 66–76.
[58] N. Funk, M. Vera, L.J. Szewciw, F. Barthelat, M.P. Stoykovich, F.J. Vernerey, Bioinspired fabrication and characterization of a synthetic fish skin for the protection of soft materials, ACS Appl. Mater. Interfaces 7 (2015) 5972–59783.
[59] S.K. Gosh, D. Mandal, High-performance bio-piezoelectric nanogenerator made with fish scale, Appl. Phys. Lett. 109 (2016) 103701.